Semi-magic Numbers from Sub-shell Closures in Shell Model Energy Levels

Shikha Awasthi[1], O.S.K.S Sastri[1] & Vandna Luthra[2]

[1]Department of Physical and Astronomical Sciences
Central University of Himachal Pradesh, HP 176215, Bharat(India)
[2]Department of Physics, Gargi College, Delhi University, Bharat(India)
[1]sastri.osks@hpcu.ac.in

Submitted on January 25, 2025

Abstract

The magic numbers associated with shell closures at the β-stability line are a well-established concept. The experimental observation of highly neutron-rich nuclei, such as ^{24}O, ^{42}Si, and ^{54}Ca, exhibiting remarkable stability has inspired a search for new magic and semi-magic numbers based on sub-shell closures. The purpose of this work is to guide graduate-level students in analyzing possible sub-shell closures that could result in magic and semi-magic numbers [1], based on the single-particle energy states of the nuclear shell model. The analysis focuses on doubly magic nuclei near the β-stability line, ranging from $^{16}_{8}$O to $^{310}_{126}$X, by classifying them into various categories-light, medium, heavy, and super-heavy nuclei; to deduce potential magic and semi-magic numbers for neutron number (N) and proton number (Z) [2]. The stability of nuclei with $N = 14, 34, 40$ and $Z = 14, 34$ has been confirmed, while nuclei with $N = 6, 16, 18, 32, 58, 64, 92, 100, 136, 164$, and 172, as well as $Z = 18, 58$, and 76, are predicted to exhibit stability. This analysis is particularly helpful for undergraduate (UG) students to understand why gaps exist between energy levels according to the single-particle shell model scheme.

Keywords: Magic and Semi-magic numbers, Doubly magic nuclei, Shell model, Central Divided Difference (CDD) Method, Gnumeric.

1 Introduction

It is a well-known fact that the atomic nuclei exhibit similar shell structure as that of atomic shells with neutrons and protons forming the shells. These discrete shells are the quantum states of neutrons and protons which are most important in understand-

ing the structure of a nucleus. The large gaps between these single particle energy states exists when there is a shell closure at N or Z equal to 2, 8, 20, 28, 50, 82, 126 and 184 (for neutrons only) i.e the so called 'magic numbers'. The nuclei which have either proton or neutron equal to magic number are known as 'magic nuclei' and the nuclei which have both proton and neutron equal to magic number are known as 'doubly magic nuclei'. Due to the shell gaps in energy states for filled shells at different magic numbers, the nucleons are more tightly bound to the nucleus causing extra stability to the nucleus as compared to the adjacent nuclei [3]. Also magic nuclei are less deformed as compared to their neighbouring nuclei. This results in abundance of elements with neutron number (N) = magic number. But in recent years, the studies have revealed that in some cases the usual shell closures disappear and the new shell closures appear [4], [5]. The appearance and disappearance of these Magic numbers may depend on different mass regions under consideration. The discovery of new magic numbers [6] may help in deciding the existence limit of Superheavy nuclei [7]. Many Magic and Semi-Magic numbers are predicted theoretically [ptu] and experimentally e.g ${}^{24}_{8}O$, ${}^{42}_{16}Si$, ${}^{54}_{20}Ca$ etc. [8, 9, 10] by many groups using separation energy plots, pairing energy plots, binding energy investigations and by using different methods such as Hartree-Fock-Bogoliubov methods [11].

The syllabus of graduate level [12, 13, 14] includes Nuclear Shell model and magic numbers, but it will be easy for students to grasp the essence of how energy levels of different nuclei are formed and how are magic numbers obtained from them. In this work, we are trying to deduce magic and semi-magic numbers using single particle energy states of neutron and proton [1] for doubly magic nuclei from ${}^{16}_{8}O$ to ${}^{310}_{126}X$ in quite an easy manner which is within the approach of graduate level students. This will provide a better understanding for graduate level students about how the single particle energy levels are formed within a nucleus according to nuclear Shell model and also how the magic numbers can be realised from them. Neutron and proton single-particle energy states were determined by solving the time-independent Schrödinger equation, with the Woods-Saxon potential [15] serving as the mean-field. The obtained energy states for neutrons and protons are used to predict the Magic and Semi-Magic numbers by calculating the gaps between the states. The Shell model [3] is very effective model to obtain the ground state energies for all nuclei. The motivation behind this work is how many Magic and Semi-Magic numbers can be deduced by using the single particle energy states for various neutron number (N) and proton number (Z).

In the following section, we present a brief overview of the simulation methodology proposed by D. Hestenes [16], which utilizes the numerical matrix diagonalization technique [17] to determine the single-particle

energy states of neutrons and protons in doubly magic nuclei [18]. Section 3 provides the simulation results along with a detailed discussion. Finally, Section 4 summarizes our conclusions.

2 Simulation Methodology

2.1 Modeling the interaction using Woods-Saxon (WS)potential:

The interaction between nucleons is modelled using a mean field potential i.e Woods-Saxon potential or a simple rounded square well potential. The Woods-Saxon potential is able to predict some magic numbers, but inclusion of Spin-orbit potential is necessary to obtain the entire magic numbers. The Spin-orbit potential is proportional to the derivative of the mean field potential.

The modeling aids in the reduction of the two-body problem to a one-body problem, with the reduced mass of the system acquired as a bound state of the central potential, which is best expressed in spherical polar co-ordinates. The central equation governing the dynamics at the microscopic domain is the Time-Dependent Schrödinger Equation (TDSE) which through separation of variables in and t results in Time-Independent Schrödinger Equation (TISE) [18]. The radial equation governing the system for $\ell = 0$ is given by

$$-\frac{\hbar^2}{2\mu}\frac{d^2u(r)}{dr^2} + V_{eff}(r)u(r) = Eu(r) \qquad (1)$$

Now the effective potential experienced by a neutron or a proton is given by:

$$V_{eff}(r)u(r) = V_{cf}(r) + V_i(r) \qquad (2)$$

Where, $V_{cf}(r)$ is the centrifugal potential given by:

$$V_{cf}(r) = \frac{\ell(\ell+1)\hbar^2c^2}{2\mu c^2 r^2} \qquad (3)$$

Here, μ denotes the reduced mass [1], which varies between the neutron and the proton. The constant $\hbar c$ has a value of 197.327 MeV-fm.

$$\mu = \begin{cases} \frac{m_n \times (Z \times m_p + (N-1) \times m_n)}{(Z \times m_p + N \times m_n)}, & \text{for neutron} \\ \frac{m_p \times ((Z-1) \times m_p + N \times m_n)}{(Z \times m_p + N \times m_n)}, & \text{for proton} \end{cases} \qquad (4)$$

Here, $m_p = 938.272$ and $m_n = 939.565$ are masses of proton and neutron respectively, in units of MeV/c^2. $V_i(r)$ is the net interaction potential; for a neutron, $V_n(r)$ and a proton, $V_p(r)$ respectively given as:

$$V_n(r) = V_{WS}(r) + V_{\ell s}(r) \qquad (5)$$

$$V_p(r) = V_{WS}(r) + V_{\ell s}(r) + V_C(r) \qquad (6)$$

The mean-field potential is modeled as [1]:

- Woods-Saxon potential (rounded square-well potential) given by

$$V_{WS}(r) = \frac{V_0}{1 + \exp\left(\frac{r-R}{a}\right)} \qquad (7)$$

where V_0 is the depth of the well.

$$V_0 = \begin{cases} -51 + 33((N-Z)/A)\ MeV, \\ \qquad\qquad \text{for neutrons} \\ -51 - 33((N-Z)/A)\ MeV, \\ \qquad\qquad \text{for protons} \end{cases} \qquad (8)$$

Where, $R = R_0 A^{1/3}$ ($R_0 = 1.28$) is the radius of the nucleus, a is surface diffuseness parameter (taken = 0.66) [19]

- The Spin-orbit potential is given by

$$V_{ls}(r) = V_1 \left(\frac{r_0}{\hbar}\right)^2 \frac{1}{r}\frac{d}{dr}\left[\frac{1}{1+\exp\left(\frac{r-R}{a}\right)}\right] \textbf{(L.S)} \quad (9)$$

Here, the spin-orbit coupling term is given by $\mathbf{L}\cdot\mathbf{S} = [j(j+1) - \ell(\ell+1) - 3/4], \hbar^2$, where ℓ is the orbital angular momentum quantum number, $j = \ell + s$ represents the total angular momentum quantum number and s is spin angular momentum quantum number (= 1/2 for nucleons). V_1 and r_0 ($V_1 = -0.44V_0$ and $r_0 = 0.90$ [1]) are the proportionality constants.

For protons, the Coulomb interaction is included given by:

$$V_c(r) = \begin{cases} \frac{(Z-1)e^2}{4\pi\epsilon_0 r}, & \text{for } r \geq R_c \\ \frac{(Z-1)e^2}{4\pi\epsilon_0 R_c}\left[\frac{3}{2} - \frac{r^2}{2R_c^2}\right], & \text{for } r \leq R_c \end{cases} \quad (10)$$

Here, R_c denotes the nuclear charge radius, which is assumed to be $\approx$ radius of the nucleus. This potential is multiplied and divided by electron rest mass energy, $m_e c^2 = 0.511\ MeV$ to rephrase it in MeV units. The rephrased potential is given by:

$$V_c(r) = \begin{cases} \frac{(Z-1)*2.839*0.511}{r}, & \text{for } r \geq R_c \\ \frac{(Z-1)*2.839*0.511}{R_c}\left[\frac{3}{2} - \frac{r^2}{2R_c^2}\right], & \text{for } r \leq R_c \end{cases} \quad (11)$$

Equation 1 represents the Time-Independent Schrödinger Equation in the form of an eigenvalue problem, $Hu(r) = Eu(r)$, where H denotes the Hamiltonian operator. The radial wave function $u(r)$ must satisfy the boundary condition $u(0) = 0$ and decay to zero as $r \to \infty$ to ensure it is properly normalized.

2.2 Numerical Technique used :

When deciding to choose a numerical technique for implementaion, there are three crucial factors to consider i.e stability, accuracy, and efficiency. The choice of these techniques also depends on computational efforts and computational time required. In current work, we chose to work with Central divided difference technique (CDD). Due to the truncation of Taylor series to two terms, the accuracy of CDD method is of order $O(h^4)$. CDD method is the simplest and most appealing matrix diagonalisation method which can be easily implemented by students in computer.

So, the main idea behind choosing CDD technique is that we want these calculations accessible to UG level students. Working in free open source software (FOSS) like Gnumeric worksheets is a best way to make students understand the problem easily [20]. Also Gnumeric has an additional advantage as compared to other worksheet environments, to obtain eigen values by giving a simple formula '$eigen()$'.

Unlike other numerical techniques like Matrix Methods (MM) [17] using Sine basis

which can not be solved in Gnumeric worsheets due to inabilty to solve complex integrals and Numerov Matrix Method (NMM) [21], which requires more computational time and effort, CDD is simple method with three easy steps and can be easily implemented in spreadsheets. Also, since the steps to obtain eigenvalues for both MM and NMM methods are more, therefore these methods have a slightly lengthier algorithm as compared to CDD method. Hence obtaining solution through CDD method requires less computational time and effort, and therefore is a good choice for implementation in UG lab projects.

2.2.1 Central Divided Difference (CDD) Method for second order derivative:

The Taylor series expansion of a function $U(x)$ about the point x_j is expressed as follows:

$$f(x) = f(x_j) + f'(x_j)(x - x_j) + \frac{1}{2!}f''(x_j)(x - x_j)^2 + \dots \quad (12)$$

If the point x lies sufficiently close to x_j, the Taylor series converges rapidly, allowing us to retain only the leading terms. By setting $x = x_j + h$, where h is a small step size, the series can be re-expressed in terms of h as:

$$f(x_j + h) = f(x_j) + f'(x_j)h + \frac{1}{2!}f''(x_j)h^2 + O(h^3) + \dots \quad (13)$$

Similarly, the Taylor Series for a point $x = x_j - h$ would be

$$f(x_j - h) = f(x_j) - f'(x_j)h + \frac{1}{2!}f''(x_j)h^2 - O(h^3) + \dots \quad (14)$$

Adding Eqns.(13) and (14), we get

$$f(x_j + h) + f(x_j - h) = 2f(x_j) + f''(x_j)h^2 + O(h^4) + \dots \quad (15)$$

So, expressing $x_j + h$ as x_{j+1} and $x_j - h$ as x_{j-1}, second derivative for the function at point x_j is obtained as

$$f''(x_j) = \frac{f(x_{j-1}) - 2f(x_j) + f(x_{j+1})}{h^2} \quad (16)$$

accurate to $O(h^2)$.
Substituting Eq.(16) in Eq.(12) and rearranging, the wave function ψ can be determined at points x_{j+1} in au as:

$$\psi(j+1) = 2\psi(j) - \psi(j-1) - 2h^2(E - V(j))\psi(j), \quad j = 2, 3, ...N. \quad (17)$$

The wavefunction $\psi(j)$ at all values of x_j (j = 3, 4, . . . , N) can be determined by choosing appropriate values for $\psi(1)$ and $\psi(2)$, for a particular value of energy E.

2.2.2 CDD Method by taking TISE as Matrix equation:

TISE can also be expressed as a tridiagonal matrix equation by writing $N - 2$ simultaneous equations that are the result of applying Eq. (16) to all $N - 2$ intermediate

points, $j = 2, 3, ..., N-1$, within the potential well. Expressing the second derivative of the wave function for intermediate points x_j, as

$$\frac{d^2}{dx^2}\psi(x_j) = \frac{\psi(x_{j-1}) - 2\psi(x_j) + \psi(x_{j+1})}{h^2} \tag{18}$$

and substituting into Time Independent Schrödinger Equation written as eigenvalue equation

$$H\psi(x) = -\frac{\hbar^2}{2m}\frac{d^2\psi(x)}{dx^2} + V(x)\psi(x) = E\psi(x) \tag{19}$$

We obtain,

$$-\frac{\hbar^2}{2mh^2}\psi(x_{j-1}) + \left(\frac{\hbar^2}{mh^2} + V(x_j)\right)\psi(x_j) - \frac{\hbar^2}{2mh^2}\psi(x_{j+1}) = E\psi(x_j). \tag{20}$$

where E denotes the eigenvalues and $\psi(x)$ represents the corresponding eigenfunctions. By letting $V(x_j) = V_j$, $\psi(x_j) = \psi_j$, and introducing

$$f_j = \frac{\hbar^2}{mh^2} + V_j = f + V_j,$$
$$g = -\frac{\hbar^2}{2mh^2} = -f/2, \tag{21}$$

the equation simplifies to:

$$g\psi_{j-1} + f_j\psi_j + g\psi_{j+1} = E\psi_j, \quad j = 2, 3, \ldots, N-1. \tag{22}$$

Also, $\psi_1 = 0$ and $\psi_N = 0$, the following equations result for $j = 2, 3, \ldots, N-1$ as:

$$f_2\psi_2 + g\psi_3 + 0\psi_4 + \ldots + 0\psi_{N-3} + 0\psi_{N-2} + 0\psi_{N-1} = E\psi_2, \quad j = 2,$$

$$g\psi_2 + f_3\psi_3 + g\psi_4 + \ldots + 0\psi_{N-3} + 0\psi_{N-2} + 0\psi_{N-1} = E\psi_3, \quad j = 3,$$

$$\vdots \qquad\qquad \vdots$$

$$0\psi_2 + 0\psi_3 + 0\psi_4 + \ldots + g\psi_{N-3} + f_{N-2}\psi_{N-2} + g\psi_{N-1} = E\psi_{N-2}, \quad j = N-2,$$

$$0\psi_2 + 0\psi_3 + 0\psi_4 + \ldots + 0\psi_{N-3} + g\psi_{N-2} + f_{N-1}\psi_{N-1} = E\psi_{N-1}, \quad j = N-1.$$

Rewriting these equations in matrix form :

$$\begin{bmatrix} f_2 & g & 0 & \ldots & 0 & 0 & 0 \\ g & f_3 & g & \ldots & 0 & 0 & 0 \\ \vdots & \vdots & \vdots & \ddots & \vdots & \vdots & \vdots \\ 0 & 0 & 0 & \ldots & g & f_{N-2} & g \\ 0 & 0 & 0 & \ldots & 0 & g & f_{N-1} \end{bmatrix} \begin{bmatrix} \psi_2 \\ \psi_3 \\ \vdots \\ \psi_{N-2} \\ \psi_{N-1} \end{bmatrix}$$

$$= E \begin{bmatrix} \psi_2 \\ \psi_3 \\ \vdots \\ \psi_{N-2} \\ \psi_{N-1} \end{bmatrix}$$

which may be concisely expressed as

$$H_{(N-2)\times(N-2)}\psi_{(N-2)\times 1} = E\psi_{(N-2)\times 1} \tag{23}$$

In Eq. (23), the Hamiltonian matrix is a tridiagonal symmetric matrix and is solved to obtain $(N-2)$ eigen functions and their corresponding eigen functions.

2.3 Implementation in Gnumeric worksheet :

While implementing in Gnumeric worksheet, the step by step procedure to solve Woods-Saxon potential using CDD method is required. An algorithm which will help students to understand the procedure, how to obtain single particle energy states is given below in Fig.(1). In supplementary material (**Appendix 1**), the procedure to solve the given Algorithm for proton states of doubly magic nucleus $^{56}_{28}Ni$ is given in Gnumeric worksheet, which can be easily reproduced. The energy level sequence for all doubly magic nuclei starting from $^{16}_{8}O$ to $^{310}_{126}X$ can be obtained by following the procedure given in **Appendix 1**.

3 Computational Results and Interpretation

The model parameters have been obtained earlier by our group [1] by using Variational Monte Carlo (VMC) technique in tandem with Matrix method [17] and are universally applicable to all the nuclei from lighter to heavy region. The energy level sequence for all the doubly magic nuclei have been obtained by solving TISE using CDD method and is in very good agreement with our previous results using matrix Numerov method [21] and also with experimentally available data [22]. To validate our process, the comparison of numerical results (using CDD method) with our previuos results [23] along with experimental results of doubly magic nucleus $^{40}_{20}Ca$ are given in Table (2).

3.1 Categorizing the nuclei

The gap between energy levels varies depending on the mass region under consideration. For lighter nuclei, the lower magic numbers exhibit larger energy gaps. As we move toward heavier nuclei, the energy gap between the same energy levels decreases, as demonstrated in the plot of energy differences between neutron states of various doubly magic nuclei for a specific magic number (Fig. 2). This trend occurs because, in heavier nuclei, the lower energy levels become inert and are thus suppressed, reducing the gap between filled shells.

To determine the magic and semi-magic numbers from the individual single-particle energy states of protons and neutrons, the doubly magic nuclei have been categorized into distinct mass ranges: light, medium, heavy, and super-heavy. This categorization ensures that the magic numbers are derived appropriately according to the specific mass region under investigation.

A key observation from Fig. 2 is the presence of pronounced energy gaps between consecutive single-particle states, which are crucial for identifying magic numbers. According to the nuclear shell model framework [19], such gaps, typically exceeding approximately 1 MeV; indicate shell closures that correspond to magic numbers. These significant energy separations reflect enhanced nuclear stability arising

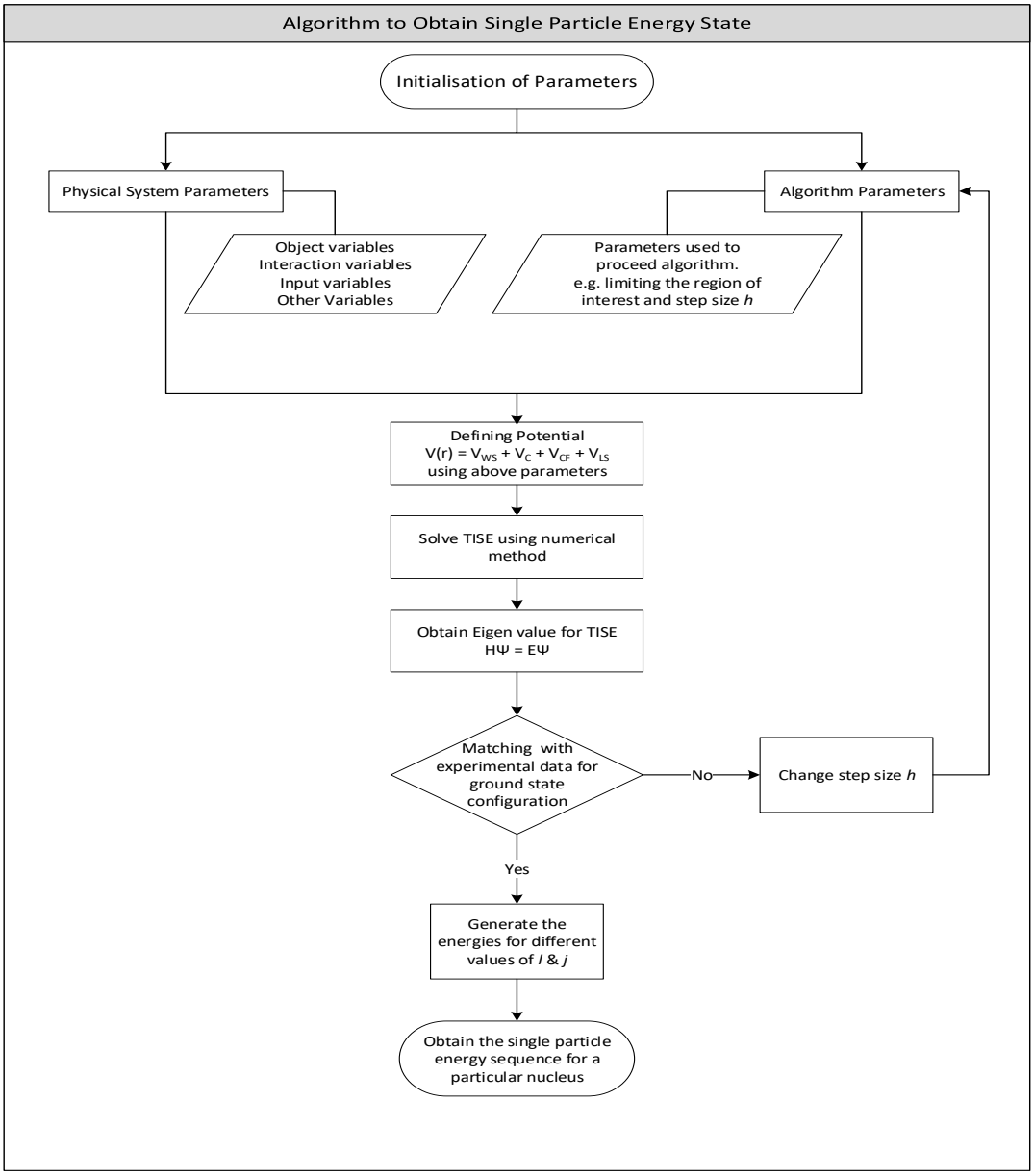

Figure 1: Algorithm to obtain single particle energy states

from filled nucleon shells, as nucleons in closed shells require a substantial amount of energy to be excited to higher states.

The energy differences between states have been calculated for both neutron and proton levels and are presented in **Appendix 2**. The plots of energy differences (in MeV) with respect to the energy level sequence for various doubly magic nuclei clearly demonstrate that at magic and semi-magic numbers, the gap between filled shells is significantly larger compared to adjacent lev-

Table 1: Comparison of single-particle energy levels (in MeV) for **protons** and **neutrons** in the doubly magic nucleus $^{40}_{20}$Ca, as obtained in the present study (*via the CDD method*), with corresponding experimental data [22] and previously reported numerical results from our group [23] (*using the Matrix Numerov method*)

States	Proton states (MeV)			States	Neutron states (MeV)		
	Exp.	Numerical values			Exp.	Numerical values	
	Ref[22]	NMM[21]	Present work		Ref[22]	NMM[21]	Present work
$1d5/2$	-15.07	-12.19	-12.19	$1d5/2$	-22.39	-19.54	-19.52
$2s1/2$	-10.92	-8.14	-8.17	$2s1/2$	-18.19	-15.54	-15.54
$1d3/2$	-8.33	-6.85	-6.85	$1d3/2$	-15.64	-14.28	-14.26
$1f7/2$	-1.09	-2.33	-2.33	$1f7/2$	-8.36	-9.15	-9.12
$2p3/2$	0.69	1.00	0.98	$2p3/2$	-5.84	-5.42	-5.42
$2p1/2$	2.38	2.94	2.93	$2p1/2$	-4.20	-3.10	-3.09
$1f5/2$	4.96	5.37	5.37	$1f5/2$	-1.56	-1.20	-1.17

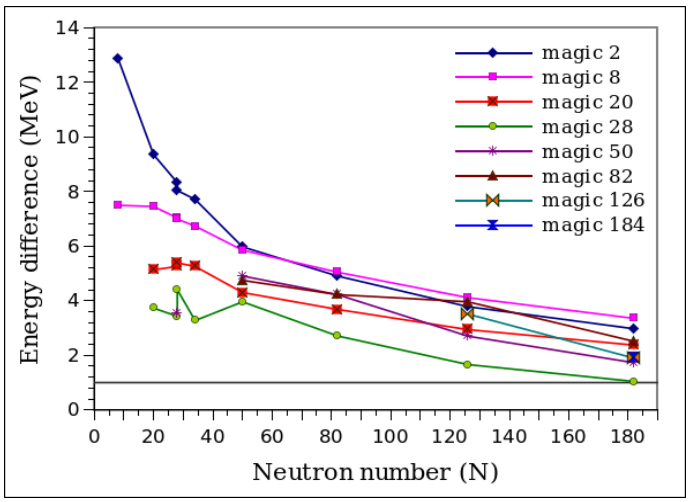

Figure 2: Energy difference vs number of neutrons for magic numbers $2, 8, 20, 28, 50, 82, 125, 184$

els. This graphical representation helps students develop a clearer understanding of the structural gaps in the energy level sequence, offering critical insights into the single-particle shell model framework.

3.2 Light nuclei : $^{16}_{8}O$ to $^{56}_{28}Ni$

Doubly magic nuclei i.e $^{16}_{8}O$, $^{40}_{20}Ca$, $^{48}_{20}Ca$ and $^{56}_{28}Ni$ in lighter mass region are very effective to study the magic numbers 2, 8, 20 and 28.

3.2.1 $^{16}_{8}O$:

If we take the case of $^{16}_{8}O$ which is at $N = Z = 8$ i.e the β-stability line, the magic numbers 2 and 8 are clearly visible for N and Z as the states $1s_{1/2}$ and $1p_{1/2}$ show the filled shells with neutron and proton equal to 2 and 8. Along with these, there is also a significant energy gap (although smaller than gap for 2 and 8) for state $1p_{3/2}$ showing 6 as the promising contender for semi-magic number.

3.2.2 $^{40}_{20}Ca$:

For $^{40}_{20}Ca$, along with magic numbers 2,8,20 for N and Z at energy states $1s_{1/2}$, $1p_{1/2}$ and $1d_{3/2}$ respectively the state $1d_{5/2}$ shows 14 as the candidate for magic number, since the energy gap is comparable to the energy gap for magic number 20. After extrapolating our data, we can also observe magic number 28 at energy level $1f_{7/2}$ for neutron states. Levels $1p_{3/2}$, $2p_{3/2}$ and $2p_{1/2}$ also shows energy gap approximately half the gap for magic numbers and predict 6 (interpolation), 32 and 34 (extrapolation) as semi-magic numbers.

3.2.3 $^{48}_{20}Ca$:

$^{48}_{20}Ca$ is another isotope of Ca having 28 neutrons and 20 protons. The magic numbers 2, 8, 20 and 28 are obtained at states $1s_{1/2}$, $1p_{1/2}$, $1d_{3/2}$ and $1f_{7/2}$ respectively for both N and Z. The state $1d_{5/2}$ shows the shell gap comparable to the state $1f_{7/2}$, again supporting 14 to be the magic number. On extrapolating the data for proton and neutron states, we get 32 as the semi-magic number with shell gap comparable to the state $1p_{3/2}$ showing 6 as the possible semi-magic number.

3.2.4 $^{56}_{28}Ni$:

$^{56}_{28}Ni$ is at the β-stability line with $N = Z = 28$. The magic numbers obtained for both neutrons N and protons Z states $1s_{1/2}$, $1p_{1/2}$, $1d_{3/2}$ and $1f_{7/2}$ are respectively 2, 8, 20 and 28. 14 is again showing its magic character at state $1f_{7/2}$. On extrapolating our data for neutron states, we get 32 as semi-magic numbers and 40 and 50 as magic number. Semi-magic behaviour of number 6 is again visible here at state $1p_{3/2}$.

3.3 Medium range nuclei : $^{100}_{50}Sn$ to $^{132}_{50}Sn$

3.3.1 $^{100}_{50}Sn$:

$^{100}_{50}Sn$ is again at β-stability line with $N = Z = 50$. On observing the energy gaps between filled shells for neutrons and protons, we get different magic and semi-magic numbers for N and Z. Magic numbers for Z = 2, 8, 18, 20, 28 and 34 are observed at states $1s_{1/2}$, $1p_{1/2}$, $1d_{3/2}$, $2s_{1/2}$, $1f_{7/2}$ and $1f_{5/2}$ respectively. For N, the magic numbers observed are 2, 8, 14, 20, 28, 50 and after extrapolation 82 magic number was also observed. Along with magic numbers, few semi-magic numbers are also observed for N = 16, 38,40, 64 and 90 and for Z = 14.

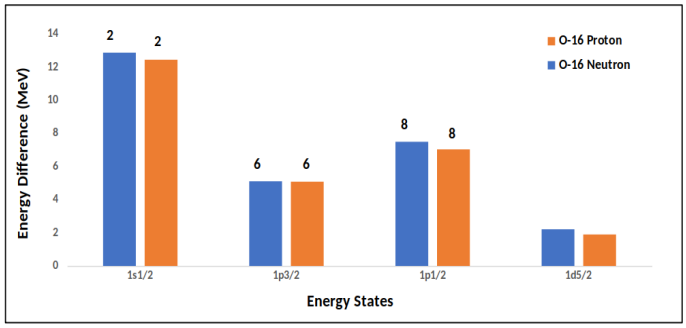

Figure 3: Separation in energy between consecutive single-particle states of $^{16}_{8}O$

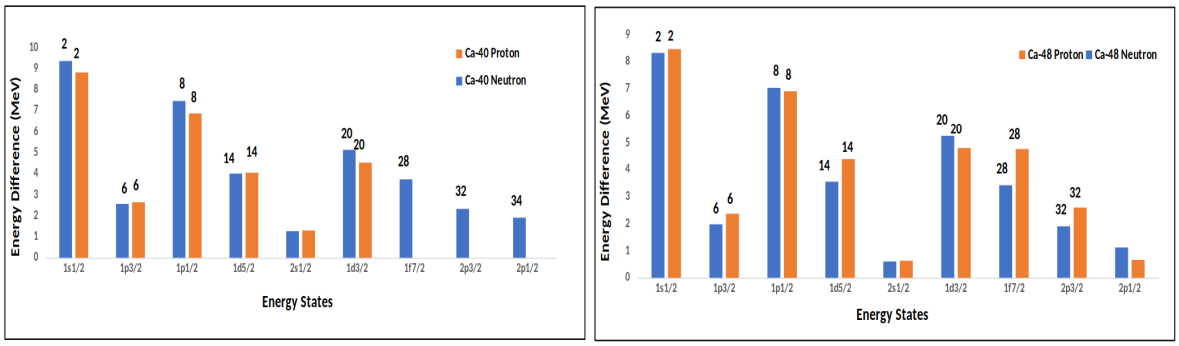

Figure 4: Separation in energy between consecutive single-particle states of (i) $^{40}_{20}Ca$ and (ii) $^{48}_{20}Ca$

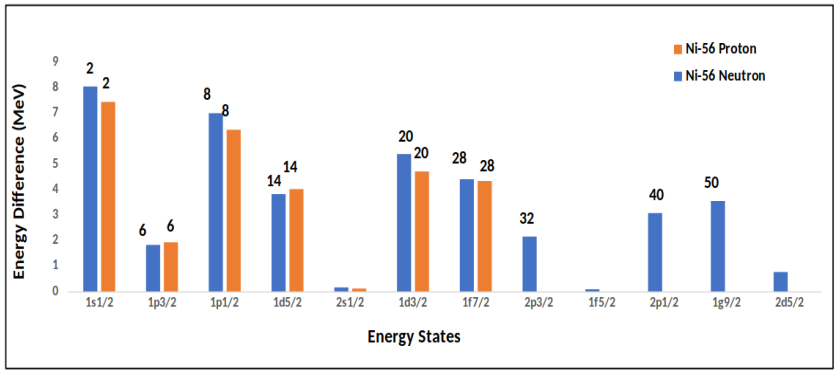

Figure 5: Separation in energy between consecutive single-particle states of $^{56}_{28}Ni$

3.3.2 $^{132}_{50}Sn$:

For $^{132}_{50}Sn$, along with already existing magic numbers 2.8. 20, 28, 50 and 82 (extrapolation), Magic number for N = 40 is observed at state $2p_{1/2}$. Semi-magic numbers for N and Z equal to 14 and 64 are observed at states $1d_{5/2}$ and $2d_{5/2}$ respectively. 18, 34 and 38 are observed semi-magic numbers for Z at states $1d_{3/2}$, 1f5/2 and 2p3/2 respec-

tively.

3.4 Heavy and Super-heavy range nuclei $^{208}_{82}Pb$ and $^{310}_{126}X$:

3.4.1 $^{208}_{82}Pb$:

The single particle neutron and proton energy states for $^{208}_{82}Pb$ show some new magic numbers. For heavy and super-heavy range, the already observed magic and semi magic numbers in the light and medium mass region are also observed for both N and Z. But here, large energy gaps are observed for magic numbers Z= 34 and 114 and N = 34, 40, 64, 100 and 126. Semi-magic numbers are observed for Z= 18, 58 and N= 18, 58, 148 and 164 (extrapolation).

3.4.2 $^{310}_{126}X$:

For $^{310}_{126}Sn$, Z= 18, 34, 58,92, 114 show large energy gaps along with already existing magic numbers. Some new magic numbers are observed at filled shells $1h_{9/2}$, $1j_{15/2}$ and $3d_{3/2}$ and $1k_{17/2}$ for N= 92, 164, 184 and 228 along with 34, 58 and 126. Semi-magic numbers are observed for Z= 76 and N=100, 136 and 172.

4 Conclusions

In this paper, an effort have been made to provide a simple procedure for students at graduate level, to understand the concept of magic and semi-magic number by analysing the energy gap between consecutive states of doubly magic nuclei ($^{16}_{8}O$ to $^{310}_{126}X$). A step wise procedure to calculate single particle energy states have also been given. Studying energy levels of doubly magic nuclei in various mass regions within the Shell model, enables to explain some of the observed sub-shell closures leading to stability in neutron rich nuclei. By calculating the energy difference or energy gap between consecutive energy states, we can deduce magic and semi-magic numbers by considering that the energy difference between two consecutive states must be greater than 1 MeV. It is observed that few numbers can be considered as the magic numbers e.g. N = 14, 34, 40, 164, 184 and 228, Z = 14, 34, 92 and 114 along with already defined magic numbers and some new semi-magic numbers can also be deduced e.g. N = 6, 16, 18, 32, 40, 58, 64, 92, 100, 136, 164 and 172, Z= 18, 58 and 76 by analysing the energy gaps between filled shells of the doubly magic nuclei. The results presented here depends only on the study done for doubly magic nuclei. The study can be further enhanced by taking more nuclei in different mass region.

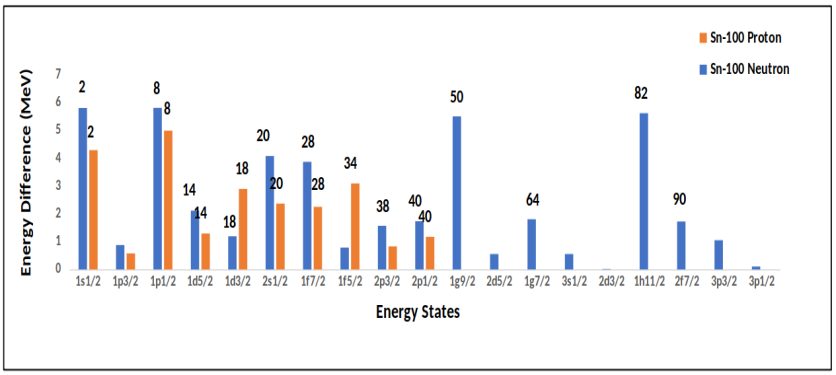

Figure 6: Separation in energy between consecutive single-particle states of $^{100}_{50}Sn$

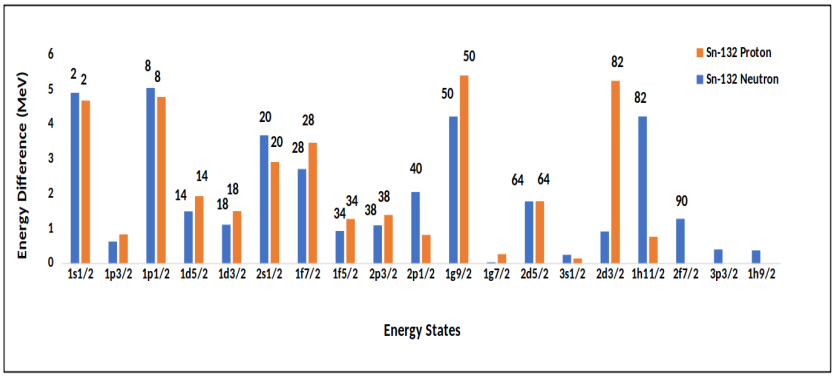

Figure 7: Separation in energy between consecutive single-particle states of $^{132}_{50}Sn$

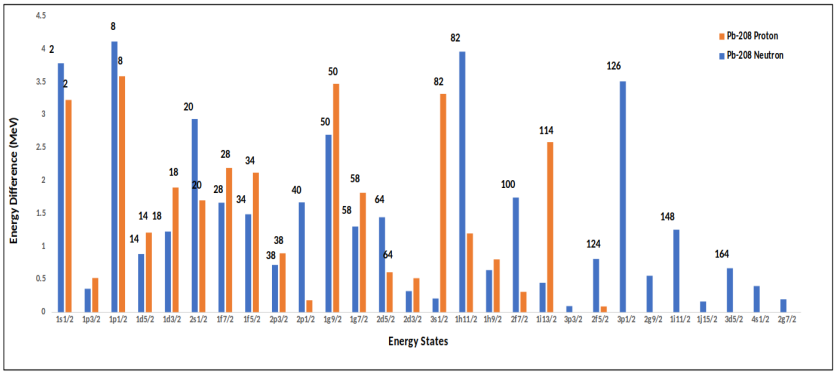

Figure 8: Separation in energy between consecutive single-particle states of $^{208}_{82}Pb$

5 Appendix 1

The various steps involved to implement Central divided difference method (CDD) in Gnumeric spreadsheets, to obtain single particle energy states of $^{56}_{28}Ni$ nucleusare given below. The Woods-Saxon potential have been taken as the as the interaction po-

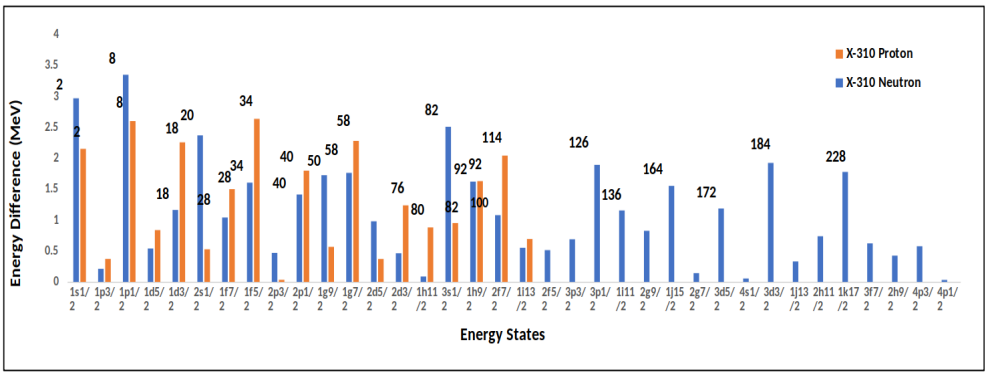

Figure 9: Separation in energy between consecutive single-particle states of $^{310}_{126}X$

tential along with spin-orbit coupling.

1. **Initialisation of parameters:** In order to initialise, we will first describe two set of parameters:
   (a) *Physical system parameters*:
   Object and interaction variables will be the inputs and state variables are the outputs, which we want to determine.
   Figure (1) shows object variables, interaction variables, algorithm variables, input variables and other variables required for the calculations.
   (b) *Algorithm parameters* The discretization of continuous variables and the reduction of infinitely large amounts to finite values, such as region of interest, provide algorithmic parameters. The step size is chosen as $h = 0.1$ and is given in cell F16, shown in Figure (10).

2. **Potential Definition:**
   The values of 'r' are generated from 0.1 to $(3 * R)$ with step-size $h = 0.1$ from A21 to A167, and to get the expected results, corresponding matrix size is 144×144. Then, four potentials are determined using the following formulae for a particular ℓ and j values. The sample sheet has been given in Figure (11)
   (a) Centrifugal potential V_{CF}, in cell B21 type the formula:

```
=($I$7*($I$7+1)*$I$13^2*
 ($A21^(-2)))/(2*$I$12)
```

(b) Woods-Saxon potential V_{WS}, in cell D21 by typing the formula:

```
=$F$8*(1+$C21)^(-1)
```

(c) L.S potential V_{LS}, in cell F21 by typing formula:

```
=-$F$13*$F$12^2*$I$15*$C21*
 $E21*($F$9*$A21)^(-1)
```

where, the L.S term in cell I15 is calculated by formula:

```
=$I$8*($I$8+1)-$I$7*($I$7+1)-3/4
```

(d) Coulomb potential, for proton, is given by typing formula:

	A	B	C	D	E	F	G	H	I	J
1	**Solving Woods-Saxon potential with Spin-orbit coupling (using CDD method)**									
2	***(Ni^{56} proton)***									
3										
4	**Initialzing the Parameters**									
5	***Object variables***				***Interaction variables***			***Input variables***		
6								*To be varied for various energy states*		
7	**Mass of neutron (m_n)**	939.565	MeV/c^2		***Woods-Saxon potential***			**Orbital angular momentum qtm.no. *(l)***	2.00	
8	**Mass of proton (m_p)**	938.272	MeV/c^2		**Potential well depth (V_0)**	−51.00	MeV	**Total angular momentum qtm no. *(j)***	1.50	
9	**Radius prop. Constant (R_0)**	1.28	fm		**Surface diffuseness (a)**	0.66				
10	**Mass of nucleus (A)**	56			**Range (R)**	4.897	fm	***Other variables***		
11	**Charge of nucleus (Z)**	28			***Spin-orbit potential***					
12	**Number of neutrons (N)**	28			**Dimensionality of distance (r_0)**	0.90	fm	**Reduced mass (μ)**	914.831	MeV/c^2
13	**Z-1 (Z_p)**	27			**Dimensionality of energy (V_1)**	22.44	MeV	**$\hbar$*c**	197.329	MeV-fm
14	**Radius of nucleus (R)**	4.897104	fm					**function *f* ($=-\hbar^2*c^2/2\mu c^2$)**	−21.282	$MeV\text{-}fm^2$
15					***Algorithm parameter***			**LS term**	−3.00	
16					**Step size (*h*)**	0.10	fm	**Cut off distance (a_0=3*R)**	14.691	fm

Figure 10: Initializing the parameters for the system

	A	B	C	D	E	F	G	H
18	**Total interaction potential**							
19								
20	**r**	**V_{cf}**	**f_1**	**V_{WS}**	**f_2**	**V_{LS}**	**V_C**	**$V=V_{cf}+V_{WS}+V_{LS}+V_C$**
21	0.1	12769.1517	0.0006973	−50.964464	0.9986	0.5753	11.9961430	12730.7586429
22	0.2	3192.2879	0.0008113	−50.958655	0.9984	0.3346	11.9911401	3153.6550267
23	0.3	1418.7946	0.0009441	−50.951898	0.9981	0.2595	11.9828019	1380.0850426
24	0.4	798.0720	0.0010985	−50.944037	0.9978	0.2264	11.9711284	759.3254726
25	0.5	510.7661	0.0012782	−50.934893	0.9974	0.2107	11.9561197	471.9979694
26	0.6	354.6987	0.0014873	−50.924258	0.9970	0.2042	11.9377756	315.9163748
27	0.7	260.5949	0.0017307	−50.911888	0.9965	0.2036	11.9160963	221.8027032
28	0.8	199.5180	0.0020138	−50.897503	0.9960	0.2071	11.8910817	160.7187139
29	0.9	157.6438	0.0023432	−50.880774	0.9953	0.2141	11.8627319	118.8399115
30	1.0	127.6915	0.0027266	−50.861322	0.9946	0.2240	11.8310467	88.8852892

Figure 11: Defining potentials:

```
=$B$13*0.511*2.839*
 (3*$B$14^2-$A21^2)/(2*$B$14^3)
```

in cell G21 up-to radius 'R' of the nucleus. After that in cell G64, type the formula:

```
=0.511*2.839*$A64^(-1)*$B$13
```

which gives the Coulomb potential outside the range of nuclear radius.
(*e*) In cell H21, the net potential is determined by typing the formula as:

```
=$B21+$D21+$F21+$G21
```

3. **Obtaining Hamiltonian matrix:**
To obtain Hamiltonian matrix, we will first define two functions f_j and g: (*a*) The functions

$$f_j = \frac{\hbar^2}{mh^2} + V_j = f + V_j,$$
$$g = -\frac{\hbar^2}{2mh^2} = -f/2, \qquad (24)$$

are defined as

```
=$H21+(($I$13^2)/($I$12*$F$16^2))
```

and

```
=-(($I$13^2)/(2*$I$12*$F$16^2))
```

	A	B	C	D	E	F
1	**Hamiltonian Matrix**					
2						
3		**1**	**2**	**3**	**4**	**5**
4	**1**	16987.1425	−2128.1919	0.0000	0.0000	0.0000
5	**2**	−2128.1919	7410.0389	−2128.1919	0.0000	0.0000
6	**3**	0.0000	−2128.1919	5636.4689	−2128.1919	0.0000
7	**4**	0.0000	0.0000	−2128.1919	5015.7094	−2128.1919
8	**5**	0.0000	0.0000	0.0000	−2128.1919	4728.3819

Figure 12: Initializing the parameters for the system

in cell I21 and J21 respectively.
(*b*) Now in Sheet 2; named '*Matrix*', generate index values for rows and columns as 1 to 144 from A4:A147 and B3:EO3.
(*c*) In cell B4, type:

```
=if($A4=B$3,Initialization!$J21,
 if($A4=B$3-1,Initialization!$K21,
 if($A4=B$3+1,Initialization!$K21,0)))
```

(*d*) After that drag the formula along the row till EO3 and then downwards up-to EO147 to obtain the tridiagonal Hamiltonian matrix as shown in Figure (12).

4. **Obtaining Eigen values and Eigen vectors:**
(*a*) In Sheet 3, named '*Eigenvalues*', generate index values for rows and columns as 1 to 145 from A4:A148 and 1 to 144 from B3:EO3 to obtain matrix of size 145 × 144. The extra row has been incorporated for eigen values. Below each of the eigen values in the first row, a corresponding eigen vector of size 131 1 will be obtained.
(*b*) In cell B4, type formula

```
=eigen('Matrix'!B4:EO147)
```

After that, press three keys Ctrl+Shift+Enter altogether to obtain the required Eigen values. The result for $d_{3/2}$ state has been shown in Figure (13). The eigen value obtained is $= -10.461$.

5. **Eigen values for different states:**
The bound state energies (i.e. the energies for which eigen values are negative), are obtained for different values of ℓ and j as:
(a) For s-state, $\ell = 0$ and $j = 0.5$ corresponds to $1s_{1/2}$ state.
(b) For p-state, $\ell = 1$ and $j = 0.5, 1.5$ corresponds to states $1p_{1/2}$ and $1p_{3/2}$.
The same procedure is repeated for d, f, g, h, i etc. states to obtain all energy states till any bound state is available.

	A	B	C	D	E	F	EL	EM	EN	EO
1		**Eigen Values (MeV) and eigen vectors**								
2										
3		**1**	**2**	**3**	**4**	**5**	**141**	**142**	**143**	**144**
4	**1**	**17456.457**	**9202.933**	**8530.565**	**8516.251**	**8509.845**	**17.953**	**10.616**	**−10.461**	**6.931**
5	**2**	0.976	−0.143	0.037	0.000	0.001	0.000	0.000	0.000	0.000
6	**3**	−0.215	−0.522	0.149	0.001	0.003	0.000	0.000	0.000	0.000
7	**4**	0.040	0.583	−0.116	−0.001	−0.002	−0.001	−0.001	0.000	0.000
8	**5**	−0.007	−0.454	0.009	0.000	0.000	−0.002	−0.001	0.001	−0.001

Figure 13: Initializing the parameters for the system

6 Appendix 2

In this section, the energy difference corresponding to neutron and proton states of doubly magic nuclei from ${}^{16}_{8}O$ to ${}^{310}_{126}X$ are given in tabular form.

- ${}^{16}_{8}O, {}^{40}_{20}Ca$:
- ${}^{48}_{20}Ca, {}^{56}_{28}Ni$:
- ${}^{100}_{50}Sn, {}^{132}_{50}Sn$:
- ${}^{208}_{82}Pb$ and ${}^{310}_{126}X$:

Table 2: Single particle energies *(in MeV)* and Energy difference (E_D) in *MeV* for neutron and proton states of doubly magic $^{16}_{8}O$ and $^{40}_{20}Ca$

$^{16}_{8}O$						$^{40}_{20}Ca$					
Neutron states			Proton states			Neutron states			Proton states		
States	Energy (*MeV*)	E_D	States	Energy (*MeV*)	E_D	States	Energy	E_D	States	Energy (*MeV*)	E_D (*MeV*)
...	...	...	...	...	...	$1f5/2$	-1.20	...	...	...	
...	...	...	...	...	...	$2p1/2$	-3.10	1.90	...	...	
...	...	...	...	...	...	$2p3/2$	-5.42	2.32	...	...	
...	...	...	...	...	...	$1f7/2$	-9.15	3.73	$1f7/2$	-2.33	...
...	...	...	...	...	...	$1d3/2$	-14.28	5.13	$1d3/2$	-6.85	4.52
$2s1/2$	-3.03	...	$2s1/2$	-0.21	...	$2s1/2$	-15.54	1.26	$2s1/2$	-8.17	1.30
$1d5/2$	-5.25	2.22	$1d5/2$	-2.11	1.90	$1d5/2$	-19.54	4.00	$1d5/2$	-12.19	4.04
$1p1/2$	-12.74	7.49	$1p1/2$	-9.14	7.04	$1p1/2$	-26.99	7.45	$1p1/2$	-19.04	6.86
$1p3/2$	-17.85	5.11	$1p3/2$	-14.23	5.09	$1p3/2$	-29.55	2.56	$1p3/2$	-21.68	2.64
$1s1/2$	-30.73	12.88	$1s1/2$	-26.68	12.45	$1s1/2$	-38.90	9.35	$1s1/2$	-30.49	8.81

Table 3: Single particle energies *(in MeV)* and Energy difference (E_D) in *MeV* for neutron and proton states of doubly magic $^{48}_{20}Ca$ and $^{56}_{28}Ni$

$^{48}_{20}Ca$						$^{56}_{28}Ni$					
Neutron states			Proton states			Neutron states			Proton states		
States	Energy (*MeV*)	E_D	States	Energy (*MeV*)	E_D	States	Energy	E_D	States	Energy (*MeV*)	E_D (*MeV*)
...	...	...	...	...	...	$3s1/2$	-0.94	...	...	...	...
...	...	...	...	...	...	$2d5/2$	-1.70	0.76	...	...	...
...	...	...	...	...	...	$1g9/2$	-5.25	3.55	...	...	...
$1f5/2$	-1.87	...	$1f5/2$	-1.71	...	$2p1/2$	-8.32	3.07	...	...	...
$2p1/2$	-3.00	1.12	$2p1/2$	-2.38	0.66	$1f5/2$	-8.41	0.09	...	...	...
$2p3/2$	-4.90	1.90	$2p3/2$	-4.98	2.60	$2p3/2$	-10.56	2.15	$2p3/2$	-1.56	...
$1f7/2$	-8.33	3.43	$1f7/2$	-9.75	4.77	$1f7/2$	-14.96	4.40	$1f7/2$	-5.89	4.33
$1d3/2$	-13.58	5.26	$1d3/2$	-14.55	4.80	$1d3/2$	-20.35	5.39	$1d3/2$	-10.60	4.70
$2s1/2$	-14.19	0.61	$2s1/2$	-15.18	0.63	$2s1/2$	-20.51	0.16	$2s1/2$	-10.71	0.11
$1d5/2$	-17.75	3.56	$1d5/2$	-19.57	4.39	$1d5/2$	-24.33	3.82	$1d5/2$	-14.72	4.01
$1p1/2$	-24.78	7.03	$1p1/2$	-26.48	6.90	$1p1/2$	-31.32	6.99	$1p1/2$	-21.06	6.34
$1p3/2$	-26.76	1.98	$1p3/2$	-28.85	2.37	$1p3/2$	-33.14	1.83	$1p3/2$	-22.99	1.93
$1s1/2$	-35.08	8.32	$1s1/2$	-37.31	8.46	$1s1/2$	-41.18	8.04	$1s1/2$	-30.42	7.43

Table 4: Single particle energies *(in MeV)* and Energy difference (E_D) in MeV for neutron and proton states of doubly magic $^{100}_{50}Sn$, $^{132}_{50}Sn$

$^{100}_{50}Sn$						$^{132}_{50}Sn$					
Neutron states			Proton states			Neutron states			Proton states		
States	Energy (MeV)	E_D	States	Energy (MeV)	E_D	States	Energy	E_D	States	Energy (MeV)	E_D (MeV)
$1h9/2$	-0.21	...	...	...	...	$3p1/2$	-0.57	...	...	...	...
$3p1/2$	-0.31	0.10	...	...	...	$1h9/2$	-0.94	0.37	...	...	...
$3p3/2$	-1.36	1.05	...	...	...	$3p3/2$	-1.34	0.40	...	...	...
$2f7/2$	-3.08	1.72	...	...	...	$2f7/2$	-2.61	1.28	$2f7/2$	-1.18	...
$1h11/2$	-8.70	5.62	...	...	...	$1h11/2$	-6.83	4.22	$2d3/2$	-6.43	5.25
$2d3/2$	-8.72	0.02	...	...	...	$2d3/2$	-7.74	0.91	$3s1/2$	-6.56	0.13
$3s1/2$	-9.27	0.55	...	...	...	$3s1/2$	-7.99	0.24	$1h11/2$	-7.32	0.76
$1g7/2$	-11.08	1.81	...	...	...	$2d5/2$	-9.76	1.78	$2d5/2$	-9.10	1.78
$2d5/2$	-11.63	0.55	...	...	...	$1g7/2$	-9.79	0.02	$1g7/2$	-9.37	0.26
$1g9/2$	-17.13	5.50	$1g9/2$	-3.06	...	$1g9/2$	-14.01	4.22	$1g9/2$	-14.77	5.40
$2p1/2$	-18.87	1.74	$2p1/2$	-4.23	1.17	$2p1/2$	-16.06	2.05	$2p1/2$	-15.58	0.81
$2p3/2$	-20.44	1.57	$2p3/2$	-5.05	0.83	$2p3/2$	-17.15	1.09	$2p3/2$	-16.97	1.39
$1f5/2$	-21.22	0.79	$1f5/2$	-8.14	3.09	$1f5/2$	-18.07	0.93	$1f5/2$	-18.24	1.27
$1f7/2$	-25.09	3.87	$1f7/2$	-10.39	2.25	$1f7/2$	-20.78	2.71	$1f7/2$	-21.70	3.47
$2s1/2$	-29.17	4.08	$2s1/2$	-12.76	2.37	$2s1/2$	-24.46	3.68	$2s1/2$	-24.61	2.91
$1d3/2$	-30.36	1.19	$1d3/2$	-15.66	2.89	$1d3/2$	-25.57	1.11	$1d3/2$	-26.11	1.50
$1d5/2$	-32.48	2.11	$1d5/2$	-16.95	1.29	$1d5/2$	-27.06	1.49	$1d5/2$	-28.04	1.93
$1p1/2$	-38.29	5.81	$1p1/2$	-21.94	4.99	$1p1/2$	-32.10	5.04	$1p1/2$	-32.83	4.78
$1p3/2$	-39.16	0.88	$1p3/2$	-22.52	0.58	$1p3/2$	-32.72	0.62	$1p3/2$	-33.65	0.83
$1s1/2$	-44.97	5.81	$1s1/2$	-26.81	4.29	$1s1/2$	-37.63	4.90	$1s1/2$	-38.33	4.68

Table 5: Single particle energies *(in MeV)* and Energy difference (E_D) in MeV for neutron and proton states of doubly magic $^{208}_{82}Pb$ and $^{310}_{126}X$

$^{208}_{82}Pb$						$^{310}_{126}X$					
Neutron states			Proton states			Neutron states			Proton states		
States	Energy (MeV)	E_D	States	Energy (MeV)	E_D	States	Energy	E_D	States	Energy (MeV)	E_D (MeV)
...	...	...	...	...	...	$3f5/2$	-1.40	...	...	...	...
...	...	...	...	...	...	$4p1/2$	-1.43	0.03	...	...	...
...	...	...	...	...	...	$4p3/2$	-2.00	0.58	...	...	...
...	...	...	...	...	...	$2h9/2$	-2.43	0.42	...	...	...
...	...	...	...	...	...	$3f7/2$	-3.05	0.62	...	...	...
...	...	...	...	...	...	$1k17/2$	-4.83	1.78	...	...	...
...	...	...	...	...	...	$2h11/2$	-5.57	0.74	...	...	...
...	...	...	...	...	...	$1j13/2$	-5.90	0.33	...	...	...
$3d3/2$	-0.82	...	...	...	...	$3d3/2$	-7.83	1.93	...	...	...
$2g7/2$	-1.01	0.20	...	...	...	$4s1/2$	-7.88	0.05	...	...	...
$4s1/2$	-1.41	0.40	...	...	...	$3d5/2$	-9.07	1.19	...	...	...
$3d5/2$	-2.07	0.67	...	...	...	$2g7/2$	-9.21	0.14	...	...	...
$1j15/2$	-2.24	0.16	...	...	...	$1j15/2$	-10.76	1.55	...	...	...
$1i11/2$	-3.49	1.25	...	...	...	$2g9/2$	-11.59	0.83	...	...	...
$2g9/2$	-4.04	0.55	...	...	...	$1i11/2$	-12.75	1.16	...	...	...
$3p1/2$	-7.55	3.51	...	...	...	$3p1/2$	-14.64	1.89	...	...	...
$2f5/2$	-8.36	0.81	$3p3/2$	-0.28	...	$3p3/2$	-15.33	0.69	...	...	...
$3p3/2$	-8.45	0.09	$2f5/2$	-0.37	0.09	$2f5/2$	-15.85	0.51	$2f5/2$	-0.31	...
$1i13/2$	-8.90	0.45	$1i13/2$	-2.95	2.58	$1i13/2$	-16.40	0.55	$2f7/2$	-2.36	2.04
$2f7/2$	-10.64	1.74	$2f7/2$	-3.26	0.31	$2f7/2$	-17.48	1.08	$1i13/2$	-3.05	0.69
$1h9/2$	-11.28	0.64	$1h9/2$	-4.26	1.00	$1h9/2$	-19.10	1.62	$1h9/2$	-4.68	1.63
$1h11/2$	-15.24	3.96	$3s1/2$	-7.57	3.32	$3s1/2$	-21.61	2.51	$3s1/2$	-5.63	0.95
$3s1/2$	-15.44	0.21	$2d3/2$	-8.09	0.52	$1h11$	-21.70	0.09	$ih11/2$	-6.52	0.88
$2d3/2$	-15.76	0.32	$1h11/2$	-9.29	1.20	$2d3/2$	-22.16	0.46	$2d3/2$	-7.75	1.24
$2d5/2$	-17.20	1.44	$2d5/2$	-9.89	0.61	$2d5/2$	-23.14	0.98	$2d5/2$	-8.13	0.37
$1g7/2$	-18.50	1.30	$1g7/2$	-11.71	1.81	$1g7/2$	-24.91	1.76	$1g7/2$	-10.41	2.28
$1g9/2$	-21.20	2.70	$1g9/2$	-15.18	3.47	$1g9/2$	-26.63	1.73	$2p1/2$	-12.21	1.80
$2p1/2$	-22.87	1.67	$2p1/2$	-15.36	0.18	$2p1/2$	-28.05	1.41	$1g9/2$	-12.77	0.57
$2p3/2$	-23.59	0.72	$2p3/2$	-16.25	0.89	$2p3/2$	-28.52	0.47	$2p3/2$	-12.81	0.03
$1f5/2$	-25.07	1.49	$1f5/2$	-18.37	2.12	$1f5/2$	-30.12	1.61	$1f5/2$	-15.45	2.64
$1f7/2$	-26.74	1.66	$1f7/2$	-20.56	2.19	$1f7/2$	-31.16	1.04	$1f7/2$	-16.95	1.50
$2s1/2$	-29.67	2.94	$2s1/2$	-22.26	1.70	$2s1/2$	-33.54	2.37	$2s1/2$	-17.47	0.53
$1d3/2$	-30.90	1.22	$1d3/2$	-24.16	1.89	$1d3/2$	-34.70	1.16	$1d3/2$	-19.73	2.26
$1d5/2$	-31.78	0.88	$1d5/2$	-25.37	1.21	$1d5/2$	-35.24	0.54	$1d5/2$	-20.57	0.84
$1p1/2$	-35.89	4.11	$1p1/2$	-28.95	3.59	$1p1/2$	-38.59	3.35	$1p1/2$	-23.17	2.60
$1p3/2$	-36.25	0.36	$1p3/2$	-29.47	0.52	$1p3/2$	-38.80	0.21	$1p3/2$	-23.55	0.37
$1s1/2$	-40.03	3.78	$1s1/2$	-32.70	3.23	$1s1/2$	-41.78	2.97	$1s1/2$	-25.70	2.15

References

[1] Aditi Sharma, Swapna Gora, Jithin Bhagavathi, and O. S. K. S Sastri, "Simulation study of nuclear shell model using sine basis", Am. J. Phys. 88, 576 (2020).

[2] Jouni Suhonen. From nucleons to nucleus: concepts of microscopic nuclear theory. Springer Science & Business Media, 2007.

[3] Eugene Meyer, "Shell model of nuclear structure," Am. J. Phys. 36, 250–257 (1968).

[4] Steppenbeck, D., Takeuchi, S., Aoi, N., Doornenbal, P., Matsushita, M., Wang, H., ... & Yoneda, K. (2013). Evidence for a new nuclear 'magic number'from the level structure of 54Ca. Nature, 502(7470), 207-210.

[5] Warner, D. (2004). Not-so-magic numbers. Nature, 430(6999), 517-519.

[6] Ali A. Alzubadi, and Redhab A. Allawi. "Investigation of the magicity in some even–even Ca isotopes by using shell model and Hartree–Fock–Bogoliubov method." Indian Journal of Physics 96, 4, 1205-1216 (2022).

[7] Nakada, H., & Sugiura, K. (2014). Predicting magic numbers of nuclei with semi-realistic nucleon–nucleon interactions. Progress of Theoretical and Experimental Physics, 2014(3).

[8] Fridmann, J., I. Wiedenhöver, A. Gade, L. T. Baby, D. Bazin, B. A. Brown, C. M. Campbell et al. "Magic'nucleus 42Si." Nature 435, no. 7044 (2005): 922-924.

[9] Steppenbeck, David, Satoshi Takeuchi, Nori Aoi, P. Doornenbal, Masafumi Matsushita, H. Wang, Hidetada Baba et al. "Evidence for a new nuclear 'magic number'from the level structure of 54Ca." Nature 502, no. 7470 (2013): 207-210.

[10] Janssens, Robert VF. "Unexpected doubly magic nucleus." Nature 459, no. 7250 (2009): 1069-1070.

[11] Alzubadi, Ali A., and Redhab A. Allawi. "Investigation of the magicity in some even–even Ca isotopes by using shell model and Hartree–Fock–Bogoliubov method." Indian Journal of Physics 96, no. 4 (2022): 1205-1216.

[12] `https://www.ugc.ac.in/pdfnews/7870779_B.SC.PROGRAM-PHYSICS.pdf`.

[13] Krane, S.Kenneth, *Introductory Nuclear Physics*(Jon Wiley & Sons, New York, 1988).

[14] Samuel S.M. Wong, *Introductory nuclear physics*(New Jersey: Prentice Hall, 1990).

[15] R. D. Woods and D. S. Saxon, "Diffuse Surface Optical Model for Nucleon-Nuclei Scattering". Physical Review. 95 (2): 577–578(1954).

[16] David Hestenes. "Toward a modeling theory of physics instruction." American journal of physics 55, 5, 440-454 (1987).

[17] Jugdutt, B. A., & Marsiglio, F. (2013). Solving for three-dimensional central potentials using numerical matrix methods. American Journal of Physics, 81(5), 343-350.

[18] O. S. K. S. Sastri, Aditi Sharma, Swapna Gora, and Richa Sharma. "Comparative Analysis of Woods-Saxon and Yukawa Model Nuclear Potentials." Journal of Nuclear Physics, Material Sciences, Radiation and Applications 9, 1, 73-79 (2021).

[19] Aage Bohr and Ben R. Mottelson, Nuclear Structure (World Scientific,Singapore, 1998).

[20] Aditi Sharma and O. S. K. S. Sastri, "Numerical simulation of quantum anharmonic oscillator, embedded within an infinite square well potential, by matrix methods using gnumeric spreadsheet", European Journal of Physics (2020):1-20.

[21] Mohandas Pillai, Joshua Goglio, and Thad G. Walker, "Matrix Numerov Method for Solving Schrödinger's Equation", American Journal of Physics. 80, 1017 (2012).

[22] N. Schwierz, I. Wiedenhover, and A. Volya, "Parameterization of the Woods-Saxon potential for shell-model calculations," preprint arXiv:0709.3525 (2007).

[23] Awasthi, Shikha, Aditi Sharma, Swapna Gora, and O. S. K. S. Sastri. "Numerical Simulation of Shell Model Single Particle Energy States using Matrix Numerov Method in Gnumeric Worksheet." arXiv preprint arXiv:2205.10335 (2022).